JOURNAL OF VIROLOGY, Sept. 1997, p. 6593–6602 Vol. 71, No. 9
0022-538X/97/$04.00+0

The Amino-Terminal Fusion Domain Peptide of Human Immunodeficiency Virus Type 1 gp41 Inserts into the Sodium Dodecyl Sulfate Micelle Primarily as a Helix with a Conserved Glycine at the Micelle-Water Interface

DING-KWO CHANG,* SHU-FANG CHENG, AND WEI-JYUN CHIEN

Institute of Chemistry, Academia Sinica, Taipei, Taiwan, Republic of China

Received 7 February 1997/Accepted 30 May 1997

A peptide based on the N-terminal fusion domain of gp41 of human immunodeficiency virus type 1 (HIV-1) and its tryptophan analog were synthesized to examine the secondary structure in the micellar environment. Nuclear magnetic resonance (NMR), circular dichroism and electron paramagnetic resonance experiments indicated that the gp41 fusion peptide inserted into the micelle primarily as a helix (59%), with substantial β-structure (26.7%). Deep penetration of the peptide into the apolar hydrocarbon core was supported by the results of fluorescence experiments in which the tryptophan analog exhibited a blue shift of about 30 nm in the presence of a sodium dodecyl sulfate micelle, in 1,2-dimyristoyl-*rac*-glycero-3-phosphocholine, and in 1,2-dipalmitoyl-*sn*-glycero-3-phospho-L-serine vesicular solutions. The results of spin label-attenuated ^{1}H resonance experiments show that the region C-terminal to G16, which contains a turn structure, exhibited substantial interaction with the micelle, suggesting that it lies on the surface of micelle. Molecular simulation based on data from NMR experiments revealed a flexible hinge at residues 15 and 16 (alanine and glycine, respectively) from the N terminus of the peptide located at the micelle-solution interface. The highly conserved A15-G16 dipeptide may play a role in the function of fusion domain of HIV-1 envelope glycoprotein.

Many envelope proteins including those of human immunodeficiency virus (HIV) are synthesized as a larger polyprotein precursor which is cleaved to generate surface (SU) and transmembrane (TM) proteins (27, 31). The N-terminal region of the TM proteins was implicated in the fusion of the virion or infected cell and target cell and so was termed fusion peptide. A salient feature of a number of fusion peptides is the presence of a segment of highly nonpolar conserved amino acids (2, 15). Fusion peptides are also characterized by their relatively high content of Ala and Gly residues with short side chains (15, 17).

The most thoroughly studied envelope glycoprotein is probably influenza virus hemagglutinin, which is composed of two subunits, HA1 (SU) and HA2 (TM). It has been shown that the N-terminal region of HA2, including the leucine zipper-like domain, was induced into forming a helix when the pH was lowered to 5.0, which is required for activation of viral fusion. The trimeric coiled-coil was proposed as the fusogenic conformation (6). Insertion of HA2 into the target membrane was shown by Stegmann et al. (40).

For HIV, the envelope glycoprotein gp160 is proteolytically cleaved to generate gp120 (SU) and gp41 (TM). Unlike influenza HA1 and HA2, the two subunits of HIV are associated via noncovalent bonds on the viral external surface. There is a high degree of conservation of tandom repeats of the FLG tripeptide (FLG motif), which is 7 or 8 amino acids from the N terminus (15). Substitution of the amino acids in the fusion peptide with charged residues results in abolition of syncytium formation (14). Moreover, among the glycine residues in the fusion peptide, replacement of G10 and G16 by valine completely abolished syncytium formation, mutation had a significant effect for G13 but little effect for G3, but, interestingly, enhanced syncytium formation was observed for mutations at G5 and G20 (11). G10 is part of a hydrophobic core that may be the initiation site for helix formation (8). These observations underline the importance of the structural aspects of the primary amino acid sequence of the fusion peptide.

Peptides derived from fusion peptide sequences have been used as a model of fusion proteins to study their membrane-fusing activity; influenza virus hemagglutinin has been the most widely used. Recently, a series of peptides with amino acid residues of different lengths from the gp41 fusion region have been synthesized to study the importance of different segments in stabilizing helical structure and in forming channels across the lipid bilayer (38). It was found that the FLG motif, in particular F8, was indispensable in inducing lysis of lipid vesicles. Destabilization of 1-palmitoyl-2-oleoyl-phosphatidylglycerol (POPG) liposomes and lysis of $CD4^+$ cells induced by a peptide from the N-terminal 23 amino acids of gp41 have been observed (30). The peptide appeared to exert its biological actions by inserting into the apolar portion of the lipid vesicles. There is a dispute on the mode of insertion of the fusion peptide into the membrane. Thus, it was proposed that the peptides destabilized the membranes by insertion into the membrane at a particular angle to the membrane (3). However, Gallaher et al. argued that the entire sequence of the fusion peptide was in contact with lipid, rather than being a sided helix in contact with the lipid at a shallow angle (16). A β-structure has also been reported as the secondary structure of the fusion peptide of gp41 from a Fourier transform infrared study (33).

While conformational alteration can be monitored by the above-mentioned techniques, detailed solution structure at the

* Corresponding author. Phone: 886-2-789-8594. Fax: 886-2-783-1237. E-mail: dkc@chem.sinica.edu.tw.

atomic level has been lacking. This problem can be effectively approached by multidimensional nuclear magnetic resonance (NMR) and molecular simulation techniques to investigate the peptide-membrane interactions. In addition, circular dichroism (CD) and electron paramagnetic resonance (EPR) spectroscopic techniques were used to study the structure and interaction of the fusion peptide of gp41, $gp41_{512–535}$ (LAV_{1a}; gp41-FP) in the presence of a model membrane. A sodium dodecyl sulfate (SDS) micelle was used to model the membrane bilayer in the study, because the motion of the molecule in the presence of smaller micelle is sufficiently fast to allow sharp NMR resonance peaks to be detected. Moreover, quantitative analysis of secondary structure from CD data is possible for experiments free of interference from scattering at low wavelengths, a condition satisfied only by the smaller micelles (23). Amphipathic spin label reagents which contain unpaired electron moieties at different positions along the aliphatic chains were used to determine the location of the embedded peptide in the micelle by their effect on the line shape and intensity of ^1H and ^{13}C resonances.

It was found from detailed spectroscopic and molecular simulation analyses that the N-terminal portion of gp41-FP adopted a predominantly helical structure in the apolar interior of the micelle, with a flexible A15-G16 at the micelle-water interface and significant interaction with the micelle at the C-terminal region. The possible role of the flexible A15-G16 dipeptide is briefly discussed. Further evidence of fusion peptide penetration into the hydrophobic core of the membrane was provided by large blue shifts in the tryptophan fluorescence for an analog of gp41-FP in micellar and phospholipid bilayer solutions.

MATERIALS AND METHODS

Sample preparation. A peptide corresponding to the N-terminal domain of gp41 (AVGIGALFLGFLGAAGSTMGARS, gp41-FP) and its tryptophan derivative (AVGIGALWLGFLGAAGSTMGARS, gp41-FP-W8) were synthesized in automated mode by a solid-phase synthesizer (model 431A; Applied Biosystems, Foster City, Calif.), with 9-fluorenylmethoxycarbonyl (Fmoc) chemistry. The peptides were cleaved from the resins with trifluoroacetic acid and purified by reverse-phase high-pressure liquid chromatography on a C_{18} column. The primary sequence of the peptides were ascertained by an electrospray mass spectrometry as well as amino acid analysis.

The spin-label reagents 12-doxyl-stearic acid (12-DXSA) and 5-doxyl-stearic acid (5-DXSA) were purchased from Sigma (St. Louis, Mo.) while 1,2-dimyristoyl-*rac*-glycero-3-phosphocholine (DMPC) and 1,2-dipalmitoyl-*sn*-glycero-3-phospho-L-serine (DPPS) were obtained from Calbiochem (La Jolla, Calif.). SDS was obtained from Boehringer (Mannheim, Germany), and d_{25}-SDS was obtained from Cambridge Isotope (Andover, Mass.). These chemicals were used in the experiments without further purification. Solutions containing vesicles were prepared by solubilizing the lipids in a chloroform-methanol (4:1, vol/vol) mixture and drying the sample under a nitrogen stream before dissolving them in buffered solutions. The sample solutions were sonicated for 0.5 and 1 h, respectively, before and after the peptides were added.

gp41-FP and gp41-FP-W8 were incorporated into SDS micelles by mixing the peptides with appropriate amount of SDS in aqueous solution. The mixture was sonicated for at least 1 h. The final concentration of the peptide used in NMR experiments was 1 to 2 mM, and that of SDS was 20 to 100 mM.

EPR experiments. EPR experiments were conducted on a Bruker EMX-10 spectrometer. The X-band, first-derivative absorption EPR spectra were obtained with the following parameters: microwave frequency, 9.8 GHz; microwave power, 20 mW; total sweep width, 80 G. A 0.2 to 0.4 mM concentration of each of the two spin-label reagents, 5- and 12-DXSA was introduced into micellar solution in the presence or absence of gp41-FP. A 300-μl aliquot of peptide-SDS solution was loaded in a flat cell, which confines the water-containing sample to a space of 0.3 mm. The rotational correlation time was calculated from the formula (5, 7) $\tau_r = K \cdot \Delta H_0 \cdot [(h_0/h_{-1})^{1/2} + (h_0/h_1)^{1/2} - 2]$, where $K = 6.5 \times 10^{-10}$ s is dependent on the anisotropic hyperfine coupling values and the g-tensor terms, ΔH_0 is the line width, and h_0, h_1, and h_{-1} are the heights of the mid-field, low-field, and high-field absorption peaks, respectively.

NMR experiments. The NMR measurements were carried out on a Bruker AMX-500 spectrometer with spectral width 5,000 Hz. The carrier frequency was set to the HOD signal that was suppressed by a soft presaturation pulse or WATERGATE (21, 35). All two-dimensional spectra were recorded in the pure absorption mode by applying the time-proportional–phase-incremental (TPPI) method (29, 37). Total correlated spectroscopy (TOCSY) experiments (4, 10) were performed with a clean MLEV-17 spin-locking pulse with a mixing time of 100 ms. For through-space spin interactions, nuclear Overhauser spectroscopy (NOESY) (1, 21, 23) was performed with a mixing time of 250 or 350 ms. For the TOCSY and NOESY experiments, 512 free induction decays of 2,000 data points with 64 to 128 scans for each free induction decay were collected. The amide deuterium-proton exchange experiments (13) were carried out at 288 K after extensive lyophilization with pure H_2O. The measurements were started immediately after addition of pure (99.98%) D_2O. To determine the location of gp41-FP in the micelle, the attenuation of integrals of ^1H TOSCY cross peaks in the presence of the spin label containing unpaired electron was measured to monitor the line-broadening effect along the residues of the peptide.

^{13}C NMR spectra were acquired at 305 K on the same AMX-500 spectrometer operating at 125.76 MHz to investigate the incorporation of the spin labels in the micelle. A total of 1,024 FID transients were collected with a flip angle of 30° and a recycle delay of 2 s for all the ^{13}C experiments in solutions containing 100 mM SDS.

The data were processed by applying a Gaussian window function in the F2 dimension and a 45° or 60° shifted sine-bell window function in the F1 dimension on a Silicon Graphics Indigo workstation with XWIN-NMR software. Zero filling to 1k in F1 and to 2k to 4k in F2 was performed on all the TOCSY and NOESY data. All chemical shifts were externally referenced to the methyl resonance of 4,4-dimethyl-4-silapenta-1-sulfonate (DSS; 0 ppm).

The NOESY data were converted into interproton distance by using the 2H/3H cross peak of the aromatic ring of phenylalanine as a reference. A variation of 0.6 to 1.0 Å in the structural computation was permitted depending on the distance.

Broadening of ^{13}C and ^1H resonances by 5- and 12-DXSA occurs via dipolar-dipolar interaction of these nuclei with the unpaired electron of the spin label. The extent of broadening is inversely proportional to the distance between the interacting nucleus and the spin label raised to the sixth power (39). Thus, the method is a sensitive probe for magnetically active nuclei such as ^1H, ^{13}C, and ^{31}P.

CD experiments. For CD measurements, in general, a cell with a 1-mm path length was used for experiments with 20 μM peptide, but a cell path length of 0.1 mm was used for the experiments which required 0.2 mM peptide. A concentration of 2 mM DMPC or DPPS was used for experiments in vesicular solutions. The samples were adjusted to pH 7.0 with sodium phosphate buffer. All CD experiments were carried out on a Jasco 720 spectrometer at 298°K. Each of the CD data was obtained from an average of five scans with step resolution of 0.05 nm and band width of 1 nm. The spectra were recorded from 190 to 270 nm at a scanning rate of 50 nm/min with a time constant of 2 s. Data used in predicting the secondary-structure content were acquired with a scanning rate of 1 nm/min and a time constant of 16 s.

The secondary-structure content of the peptide can be estimated by converting observed ellipticity (θ) into mean residue ellipticity (degrees per square centimeter per decimole) by using the following equation $[\theta] = \theta \cdot l^{-1} \cdot c^{-1} \cdot N^{-1}$ where l is the cell length in mm, c is the molar concentration, and N is the number of amino acid residues in the peptide. Quantitative prediction of the secondary structure was performed by fitting CD data in the 178- to 250-nm range by the Hennessey-Johnson method (20) with 33 proteins of known secondary structure from X-ray crystallographic studies as the basis set.

Fluorescence measurements. All the fluorescence experiments were performed on a Jasco FP-777 spectrofluorometer at ambient temperature. An excitation wavelength of 280 nm was used to record spectra from 300 to 500 nm with a data interval of 0.1 or 0.2 nm. The response time was set at 1 s with a scan rate of 50 nm · min^{-1}. Excitation and emission slits of 5 and 1.5 nm, respectively, were used for measurements of gp41-FP-W8 in the presence and absence of SDS micelles (or phospholipid vesicles).

Structure computation. A total of 384 NMR-derived constraints including 19 torsional constraints and 103 nonsequential distance constraints were used in structure computation by distance geometry and simulated annealing (SA) methods (19, 34) implemented in a software package including InsightII/Discover and NMRchitect program (version 2.3) from Biosym Technologies, Inc. In the SA protocol, the temperature was raised to 800 K and a molecular dynamics run was carried out for 4 ps to allow more conformational space to be explored. The system was subsequently annealed to 300 K in 10 steps for a total of 30 ps and minimized by the steepest-descent and conjugated-gradients methods before final refined three-dimensional structures were obtained. The total internal energy was evaluated as the sum of bond, bond angle, dihedral, out-of-plane, electrostatic, and van der Waals energies. Lennard-Jones 6-12 terms were used to evaluate van der Waals energy except in the initial stage of SA, where the Lennard-Jones terms were replaced with a quadratic term to facilitate the crossover of atoms to the "correct" configuration.

RESULTS

^1H NMR data indicate that the central region of gp41-FP adopts helical structure in an SDS micellar solution. Figure 1 displays the NOESY spectra of the gp41-FP in the presence of

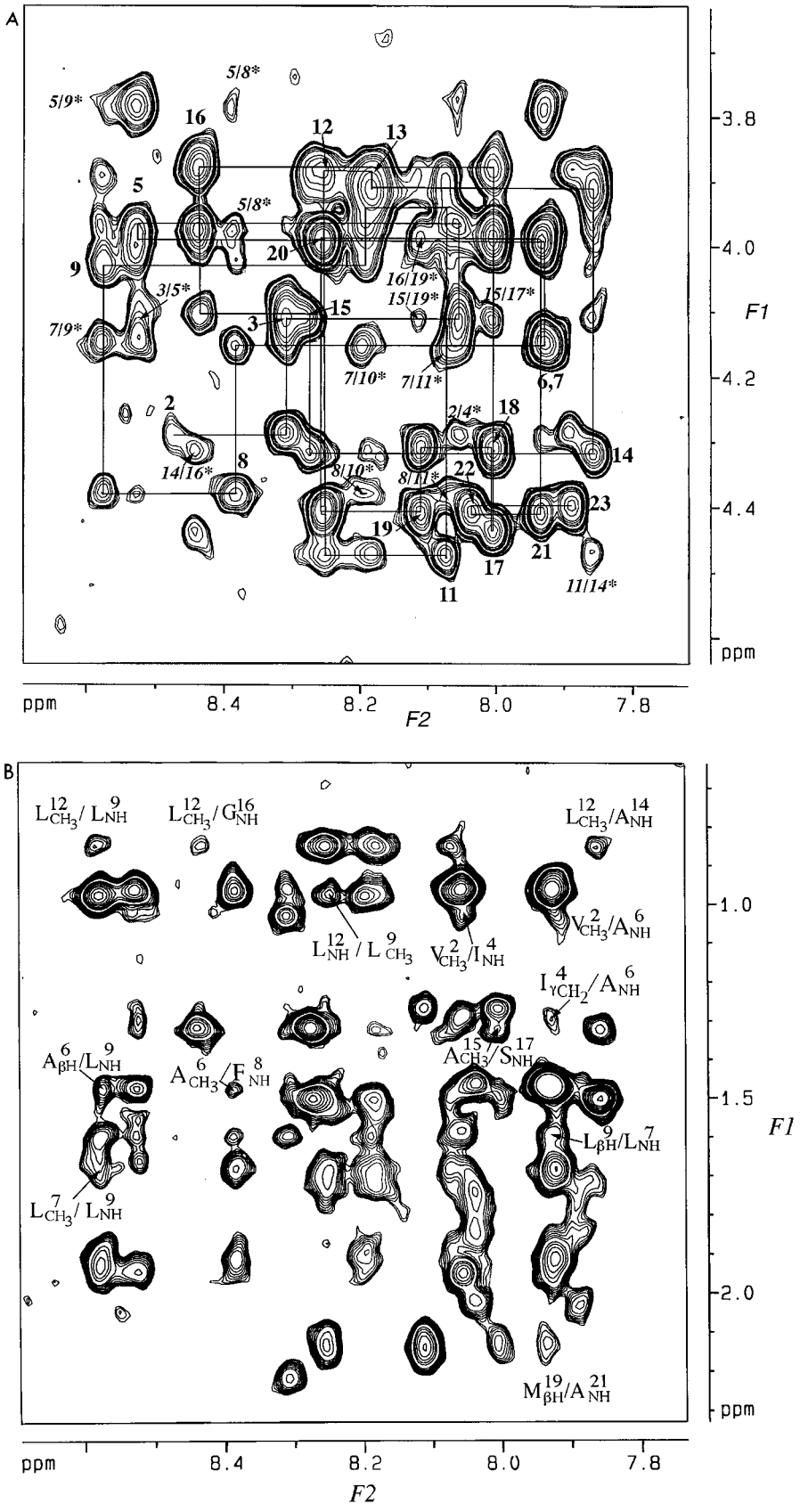

FIG. 1. Backbone NH/αH (A) and side-chain/NH (B) regions of the NOESY spectrum of 1 mM gp41-FP in 150 mM SDS micellar solution at 293 K and pH 7.0 with a mixing time of 350 ms. Sequential connectivity and representative nonsequential NOE interactions are indicated.

TABLE 1. Chemical shifts of 1 mM gp41-FP in 150 mM SDS micellar solution at 293 K and pH 7

Residue	Chemical shift of:			
	NH	αH	βH	Others
Ala1			1.55	
Val2	8.48	4.29	2.22	γCH_3: 1.04, 1.04
Gly3	8.31	4.11, 4.11		
Ile4	8.06	3.97	1.95	γCH_2: 1.28, 1.61; γCH_3: 0.96; δCH_3: 0.96
Gly5	8.53	4.00, 3.80		
Ala6	7.93	4.14	1.46	
Leu7	7.92	4.17	1.91, 1.91	γH: 1.69 δCH_3: 0.95, 0.95
Phe8	8.39	4.39	3.30, 3.30	2,6H: 7.26; 3,5H: 7.30; 4H: 7.32
Leu9	8.58	4.04	1.91, 1.91	γH: 1.61; δCH_3: 0.98, 0.98
Gly10	8.20	3.96, 3.89		
Phe11	8.07	4.48	3.27, 3.27	2,6H: 7.25; 3,5H: 7.31; 4H: 7.32
Leu12	8.25	3.89	1.74, 1.74	γH: 1.53; δCH_3: 0.86, 0.86
Gly13	8.18	3.93, 3.93		
Ala14	7.86	4.32	1.50	
Ala15	8.28	4.12	1.32	
Gly16	8.44	3.98, 3.88		
Ser17	8.01	4.44	3.99, 3.99	
Thr18	8.01	4.32	4.32	γCH_3: 1.27
Met19	8.12	4.41	2.14, 2.14	γCH_2: 2.64, 2.62; εCH_3: 1.46
Gly20	8.26	4.00, 4.00		
Ala21	7.94	4.40	1.47	
Arg22	8.04	4.39	2.02, 1.85	γCH_2: 1.76, 1.76; δCH_2: 3.26, 3.26; NH: 6.90, 6.52
Ser23	7.89	4.30	3.89, 3.89	

an SDS micelle at 293 K. Strong and contiguous $d_{NN}(i, i + 1)$ interactions as well as numerous $d_{\alpha N}(i, i + 3)$ NOE cross peaks indicate the formation of helical structure for the peptide in the hydrophobic micellar environment (44). Furthermore, except for the N-terminal residues, weaker sequential $d_{\alpha N}(i, i + 1)$ NOE interactions than those of the intraresidue $d_{\alpha N}(i, i)$ suggest the existence of primarily helical instead of β-strand or disordered structure for the peptide. In contrast, a rigid turn with little helical content was detected for the peptide in aqueous solution (8). The chemical shifts of the ^{1}H resonances are presented in Table 1, and NOE interactions are shown in Fig. 2 for gp41-FP in the SDS micellar solution. Figure 3 summarizes the chemical shift deviation of αH and βH from the random-coil values for each of the amino acids in the peptide. From the upfield shift of αH and the downfield shift of βH, it is clear that the region spanning residues 5 through 16 assumes a helical form (43), in agreement with the NOE data.

CD data of gp41-FP indicate a significant induction of helix in association with SDS micelle and phospholipid vesicles. Far UV-CD spectra of gp41-FP in aqueous and SDS DMPC/DPPS solutions are displayed in Fig. 4. Helical form is induced in the membranous environment. The helicity appears to correlate with a negative charge on the head group of lipid molecules. A similar CD profile was reported by Rafalski et al. (36) for gp41-FP in POPG vesicular solution with a high lipid-to-peptide (L/P) ratio (200:1). Figure 5 shows the result of analyzing the secondary structure of the peptide by fitting the observed CD data with reference spectra by using Hennessey-Johnson algorithm. The secondary-structure content is as follows: helix, 58.9%; β-sheet, 11.4%; β-turn, 15.3%; others, 15.3%. It is notable that the result reveals a significant β-turn population in the SDS solution.

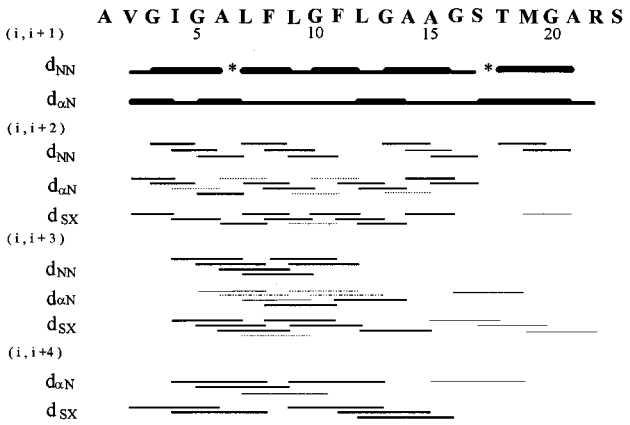

FIG. 2. Summary of ^{1}H NOE interactions for gp41-FP in the presence of SDS micelles. $d_{NN}(i, j)$ and $d_{SX}(i, j)$ denote observed NOE interactions between the backbone amide protons of residues i and j and interactions involving the side chain proton of residue i and the proton of residue j, respectively. Other NOE interactions are represented similarly. Potential NOE interactions from the overlapping cross peaks are indicated by dotted lines. Asterisks for $d_{NN}(6, 7)$ and $d_{NN}(17, 18)$ indicate unobservable cross peaks due to the closeness in the chemical shifts for these two pairs of amide protons. The thickness of the lines is approximately proportional to the peak intensity. Helical structure is characterized by $d(i, i + 3)$ and $d(i, i + 4)$ NOE peaks.

Insertion of gp41-FP in the SDS micelle and phospholipid solutions is shown by fluorescence as well as EPR experiments. To demonstrate the immersion of gp41-FP in the micellar interior by fluorescence spectroscopy, F8 was substituted by fluorescent tryptophan. The fluorescence of gp41-FP-W8 in aqueous and SDS micellar solutions and solutions containing DMPC and DPPS vesicles are presented in Fig. 6. All the emission peaks of tryptophan in the micellar and vesicular solutions exhibit a blue shift of approximately 30 nm compared to that in the aqueous solution. Blue shifts of less than 20 nm (from 352 to above 333 nm) have been observed for the association of melittin and the fusion peptide of influenza virus hemagglutinin with phospholipid bilayers (9, 12). The side chain of tryptophan in the fusion domain of influenza virus hemagglutinin has been shown to penetrate into the hydrocarbon interior of the bilayer at least 7 Å from the vesicular surface (9). The fluorescence peak for gp41-FP-W8 in the presence of model membranes (micelles and vesicles) occurs at a 10-nm-shorter wavelength than that in melittin-vesicle or HA2-vesicle complexes, indicating the fluorophore in gp41-

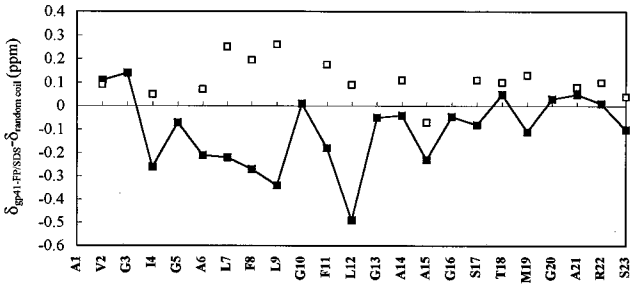

FIG. 3. Difference in the observed chemical shifts of αH (solid squares) and βH (open squares) from those of the random-coil values versus residue number for gp41-FP in the SDS micellar solution. Negative values indicate an upfield shift. The helical structure is characterized by an upfield shift in αH and a downfield shift in βH. Chemical shifts were taken from the values measured at 293 K. The data indicate a stable helical form for the segment I4 to A14.

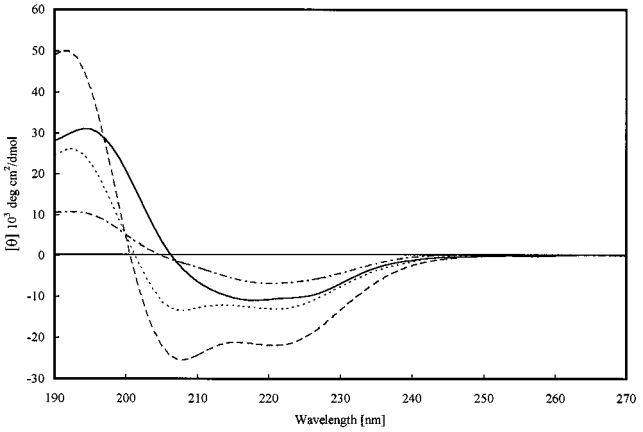

FIG. 4. CD spectra of gp41-FP in aqueous (–·––·–), SDS (L/P = 40 mM/0.2 mM) (– – –), DPPS-DMPC (DPPS/DMPC/P = 0.5 mM:1.5 mM:20 μM) (——), and DPPS-DMPC (DPPS/DMPC/P = 1.5 mM:0.5 mM:20 μM) (·····) solutions. The molar ratios of peptide to the molecules constituting the micelles and vesicles were kept at 1:200 and 1:100, respectively, in these experiments. Helical structure, indicated by minima at 208 and 222 nm, is induced in the micellar and vesicular solutions.

FP-W8 is in a more hydrophobic medium. Thus, it is clear that the peptide inserts into the SDS micelle and vesicles consisting of DMPC and DPPS (41).

A measure of molecular mobility, the rotational correlation time, τ_r, calculated from the EPR spectra of 12- and 5-DXSA in water and in SDS micellar solutions is shown in Table 2. An approximately fourfold increase of τ_r in the SDS solution relative to that in water for both the 5- and 12-DXSA probes is indicative of the incorporation of these probes into the micelles. A further 20% increase in τ_r as gp41-FP was added to the spin label-containing SDS micelle suggests incorporation of the peptide into the micelle.

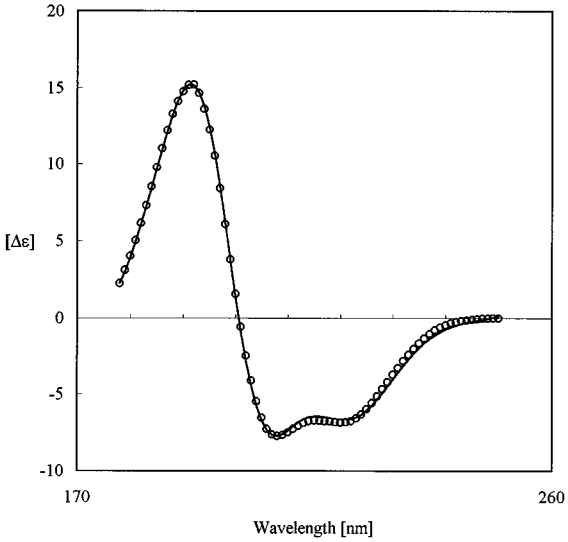

FIG. 5. Secondary-structure analysis for gp41-FP (0.2 mM) in 40 mM of SDS micellar solution from CD spectrum (solid curve) by the Hennessey-Johnson algorithm in which 33 reference CD spectra from the proteins with known crystalline structures were used. The sum of the fractions of structural components was constrained to close to 1. The best-fitting profile is represented by open circles. For an accurate secondary-structure analysis, it is essential to have reliable data at 180 nm, which is not possible in the vesicular solution owing to scattering of light as a result of the larger size of vesicles. ε is numerically equal to 1/3,299 of [θ].

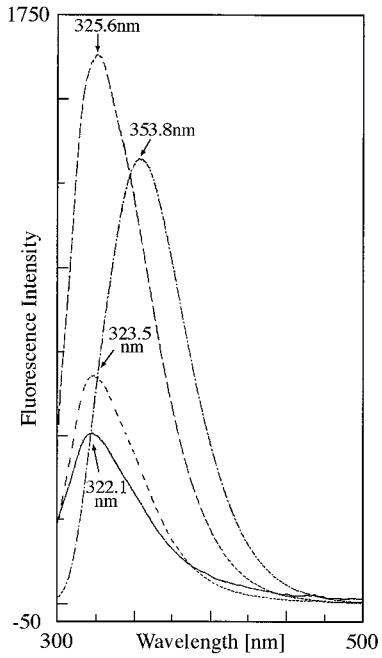

FIG. 6. Fluorescence spectra of gp41-FP-W8 in aqueous (–·––·–), SDS (– – –) (L/P = 12 mM:0.12 mM), DPPS-DMPC (DPPS/DMPC/P = 1.5 mM:0.5 mM:20 μM) (·····), and DPPS-DMPC (DPPS/DMPC/P = 1.5 mM:0.5 mM:20 μM) (——) solutions. The L/P ratio for the micellar or vesicular solution was kept at 100. The excitation wavelength was 280 nm, and the emission was scanned from 300 to 500 nm. A blue shift of the emission peak of roughly 30 nm as SDS micelles or DPPS-DMPC vesicles were introduced indicates transfer to a more hydrophobic environment for the tryptophan fluorophore.

Penetration and position of gp41-FP into the micelle is suggested by NMR using spin-label probes. Another line of evidence for the insertion of the fusion peptide of gp41 into the micellar interior is provided by the deuterium-proton exchange experiment, the result of which is displayed in Fig. 7. After 30 min of exchange, NH groups from G5 through L12 are observable, whereas after 2 h of exchange, only amide protons from F8, L9, and L12 are detectable. The results suggest that the F8-L12 stretch is deeply embedded in the micellar interior. In contrast, faster deuterium-proton exchange for residues V2-G3 and residues C-terminal to A14 suggests that these residues are near or on the surface of the micelle.

Broadening and intensity attenuation of ^1H and ^{13}C resonances by the spin label are sensitive to the distance between the interacting nucleus and the unpaired electron. Therefore, the position of the spin moiety of 5- and 12-DXSA in the micelle can be deduced from the effect of these two spin-label probes on the ^{13}C along the SDS hydrocarbon chain (24). The

TABLE 2. Rotational correlation times, τ_r, calculated from EPR spectra of spin labels in aqueous solution and SDS micellar solution in the presence or absence of gp41-FP at 298 K

System	10^{-10} τ_r (s) for:	
	12-DXSA	5-DXSA
H_2O	2.3	2.0
52 mM SDS	9.6	9.5
0.18 mM gp41-FP/52 mM SDS	11.6	11.3

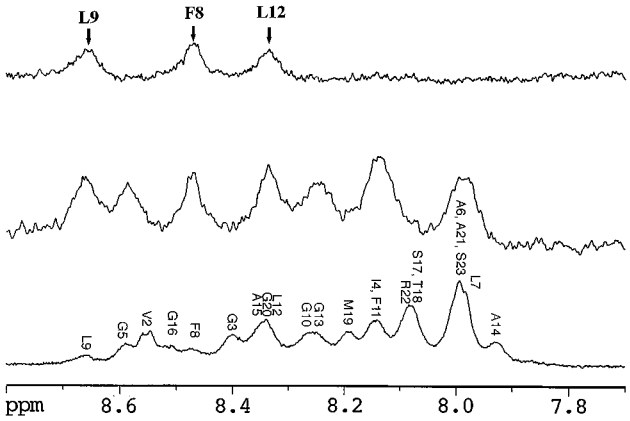

FIG. 7. The deuterium-proton exchange of gp41-FP in SDS micellar solution at 288°K. The bottom one-dimensional spectrum was acquired before the exchange experiment. The middle spectrum shows the result after 30 min of backbone NH exchange. The top spectrum demonstrates that only the amide protons in F8, L9, and L12 are still observable after 2 h of exchange, suggesting protection of the amide protons of F8 and L9 from solvent due to deep immersion in the micelle for these residues.

results are shown in Fig. 8. The more pronounced decrease by 12-DXSA of ^{13}C signals from positions 11 and 12 of SDS indicates deep immersion of the spin-label moiety in the interior of the SDS micelle. In contrast, the ^{13}C spectrum of SDS in the presence of 5-DXSA indicates that greater changes in line shape and chemical shift occur at positions close to the head group of SDS. Thus, the effects of 5-DXSA are larger at positions 1, 2, and 3 but there is no discernible effect on ^{13}C at

TABLE 3. Effect of the spin-label reagents 5- and 12-DXSA on the resonance cross peaks of the 23 residues of gp41-FP in SDS micellar solution[a]

Residue	5-DXSA				12-DXSA			
	s	ms	mh	h	s	ms	mh	h
A1			y		y			
V2			y		y			
G3			y		y			
I4				y		y		
G5	y							y
A6	y							
L7	y							y
F8	y						y	
L9	y					y		
G10	y					y		
F11	y					y		
L12		y				y		
G13	y					y		
A14	y					y		
A15		y				y		
G16				y	y			
S17		y			y			
T18		y				y		
M19		y			y			
G20		y			y			
A21		y			y			
R22		y			y			
S23		y			y			

[a] The attenuation of cross-peak intensities upon addition of spin labels is classified into four catagories: s, <40%; ms, 40 to 50%; mh, 50 to 60%; h, 60%. The gp41-FP/SDS ratio is about 1 mM/100 mM. The final concentration of spin labels in the peptide-SDS solution is 0.2 mM.

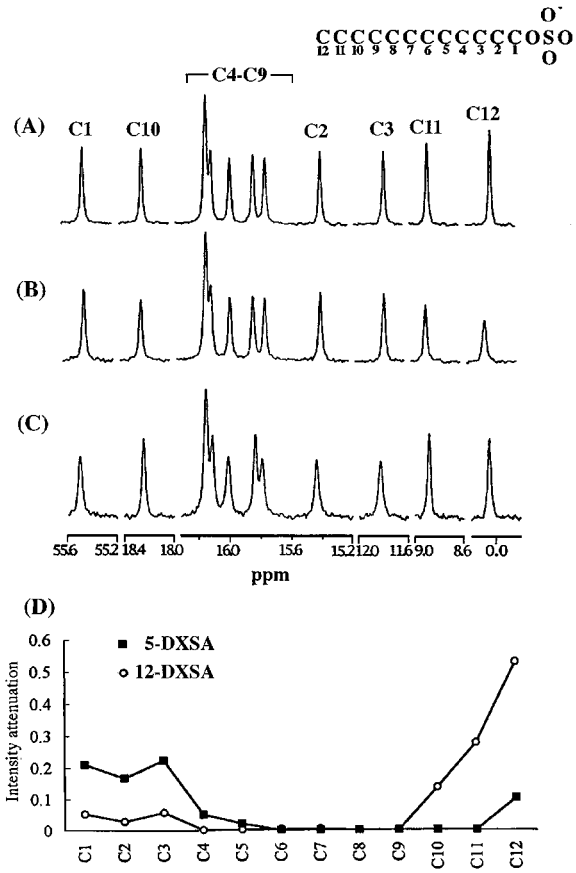

FIG. 8. (A to C) ^{13}C spectrum of 100 mM SDS (A) and resonance broadening caused by 12-DXSA (B) and 5-DXSA (C). (B and C) the spin label/SDS molar ratio is 1:80. The carbon numbering scheme of SDS is shown at the top of the figure. (D) The intensity attenuation by 5-DXSA and by 12-DXSA versus carbon number is shown in (D). No detectable change is observed for C6 through C9 by both spin labels. Note that the broadening by 12-DXSA is more pronounced for resonance peaks attributed to ^{13}C at positions 12 and 11 whereas the peaks arising from positions 1 to 3 are more affected by 5-DXSA. The results indicate that the spin-label moiety of 12-DXSA is near the center of the micelle while that of 5-DXSA is closer to the micellar surface.

positions 10, 11, and 12. The results showed that the doxyl moiety of 5-DXSA is distributed primarily near the surface of the micelle.

The location of gp41-FP in the SDS micelle, in turn, can be determined by the intensity change of the ^{1}H resonances caused by 5- and 12-DXSA. Table 3 shows attenuation of ^{1}H NOESY and TOCSY cross peaks of the peptide by the spin-label probes. The intensity reduction by 12-DXSA is largest for the segment G5 to F8, and smaller at both ends of the peptide. In contrast, the decrease in the cross-peak intensity of the peptide in the presence of 5-DXSA exhibits a different pattern. Thus, the G5 to A14 stretch shows less attenuation than do residues at the ends. Since the spin-label moiety of 12-DXSA is distributed close to the center of the micelle whereas that of 5-DXSA is closer to the surface, the result demonstrates that the FLG motif (F8 to G10) is located near the center of the SDS micelle and the N terminus is near the micellar surface. The C terminus of gp41-FP lies outside of the micelle, as the intensity reduction is generally smaller for residues at the C terminus in the presence of the two spin-label probes. The effect of 12-DXSA is illustrated in Fig. 9, in which NH/αH peaks from G5, F8, and L9 are markedly attenuated.

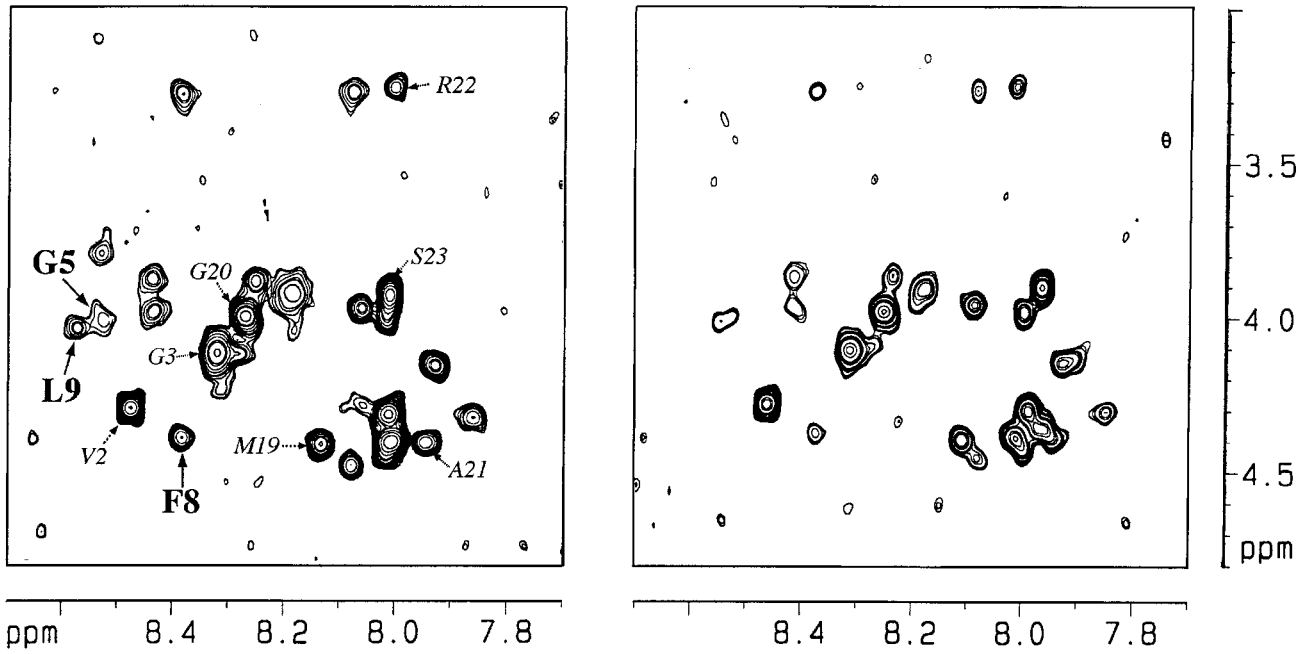

FIG. 9. Fingerprint region of the TOCSY spectra of gp41-FP in SDS solution in the absence (left) and presence (right) of 12-DXSA. The same contour levels are taken for the two spectra for comparison of intensity alteration. Higher attenuation in the intensity as a result of 12-DXSA is observed for cross peaks arising from G5, F8 and L9, which are marked in boldface. In contrast, cross peaks attributed to residues at both the N and C termini, such as V2, G3, G20, A21, R22, and S23 (italics), are attenuated to a lesser degree. This indicates that the region encompassing the FLG motif is proximal to the center of the micelle, to which 12-DXSA is close, according to the result of Fig. 8.

A schematic drawing of the peptide showing its position in the SDS micelle and interaction with the 5- and 12-DXSA probes is displayed in Fig. 10. All the molecules, including the peptide, SDS, and spin labels, are fluid, so that their relative position changes with time. The results obtained here represent the preferred distribution, and Fig. 10 depicts a representative structure.

Conformation of gp41-FP in SDS micelle solutions. Figure 11A shows superposition of 40 calculated structures for the region I4 to G20 of gp41-FP by using the DG and SA protocols with constraints derived from NMR experiments in SDS micellar solution. Figure 11B shows that the S17 to G20 stretch forms a β-turn. The average ϕ values of T18 and M19 for the 18 structures are −94° and −80°, and the average Ψ value for T18 is −57°, indicating that the turn can be described as type I. Figure 12 shows the root-mean-square deviation (RMSD) of the backbone atoms for the 40 structures shown in Fig. 11A. The structural divergence is visible for the C terminus of the peptide starting with residue G16, suggesting a flexible point at G16 for the peptide in a lipidic environment.

DISCUSSION

In aqueous solution, gp41-FP adopts a β-structure with a type I β-turn at the FLG motif region and a disordered structure at both ends (8). An α-helical structure is induced in the presence of SDS micelles, as indicated by the abundant $d(i, i + 3)$ NOE cross peaks (Fig. 2) and estimated from CD data (Fig. 4 and 5). As also found in previous studies, this structure was shown to insert into the interior of the SDS micelle in the present investigation by a variety of experiments including the H-D exchange of ^{1}H NMR, fluorescence, differential line shape change of ^{1}H NMR with 5- and 12-DXSA spin labels, whose position was determined from the ^{13}C line shape change shown in Fig. 8. The data suggest that the fusion peptide of gp41 assumes extended and disordered forms in the nonfusogenic state and transforms into a helix as it inserts into target cell membrane during fusion process. Fewer observable $d(i, i + 3)$ NOE interactions for the G16 to M19 stretch suggest a distorted helical or a less regular structure than the N-terminal region. Additionally, from the molecular simulation results (Fig. 11) the segment S17 to G20 was found to form essentially a type I β-turn which readily converts into a helical structure.

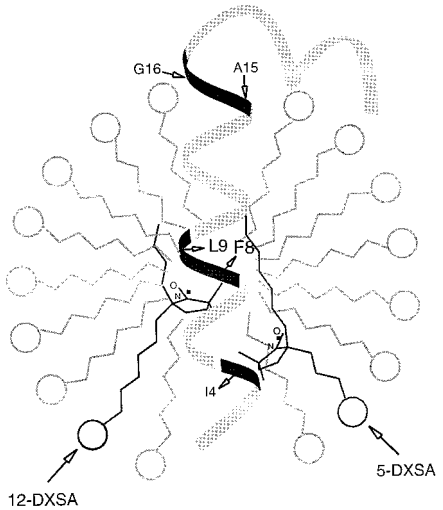

FIG. 10. Schematic drawing of the insertion of gp41-FP into the SDS micelle and its interaction with the 5- and 12-DXSA probes. A15 to G16 are depicted at the micelle-water interface, while 12- and 5-DXSA are near F8/L9 and 14, respectively. The latter result is based on the spin-label-attenuated proton resonances and proton-deuterium exchange experiments.

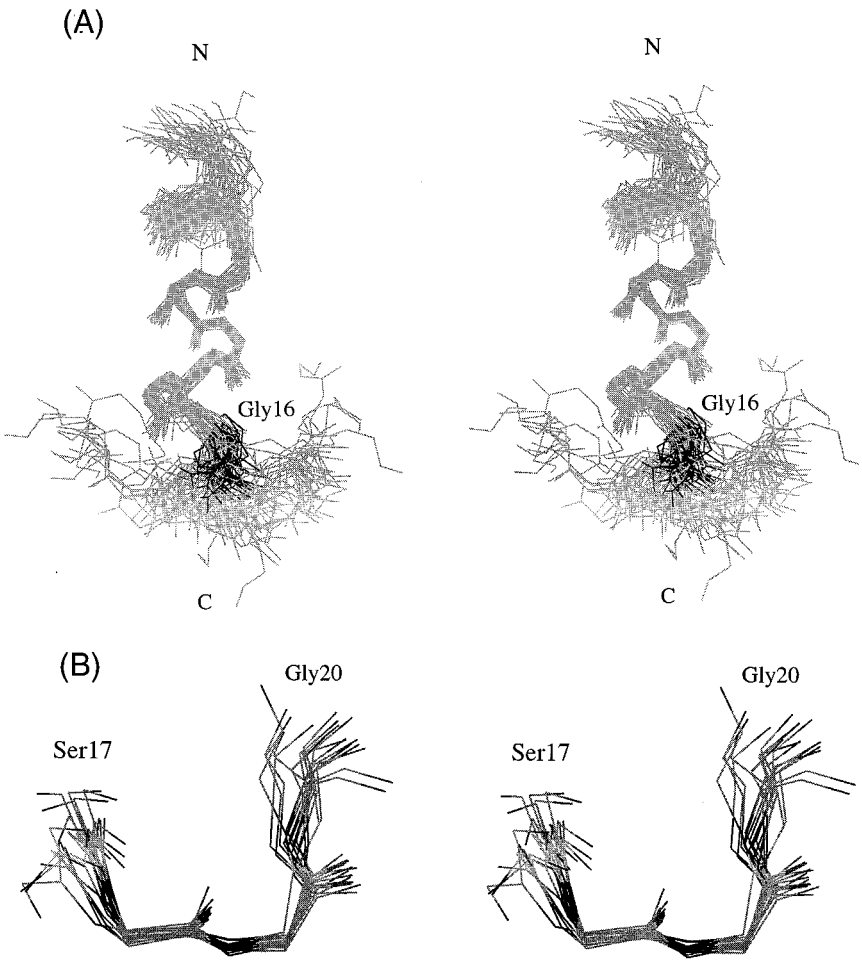

FIG. 11. Superposition of 40 structures for residues 4 to 20 (A) and 18 structures for residues 17 to 20 (B) of gp41-FP calculated by the DG and SA methods by using constraints derived from NMR experiments and hydrogen bond constraints from proton-deuterium exchange results in SDS micellar solution. G16 is marked by a darker segment in each of the structures representing gp41-FP. The divergence at the C-terminal region is visible.

The turn structure would be consistent with the prediction from the analysis of CD data (Fig. 5). The peptide representing the N-terminal 23 residues of gp41 has been shown to induce vesicle leakage and lipid mixing (36) and to cause lysis of $CD4^+$ lymphocyte (18). The varying degree of membrane disruption involved in these processes implies insertion of the fusion peptide into the membrane interior. In the present study, we showed the penetration of gp41-FP into the SDS micelle. A similar result has also been deduced by Gordon et al. (18) from an EPR study on the spin-labeled gp41-FP and by Rafalski et al. (36) from the surface tension increase caused by the peptide in the presence of POPG vesicles.

As shown in Table 3, there is a significant decrease in the intensity of ^{1}H NMR cross peaks by 5-DXSA for the residues at the C terminus of gp41-FP, suggesting their proximity to the micelle. Further, the more rapid amide proton exchange for these residues presented in Fig. 7 implies that this region of the peptide is on the exterior of the micelle. As demonstrated by the larger attenuation of amide proton resonances and the slowest exchange with deuterium, F8 and L9 are near the center of the micelle. For the NMR-derived structures, the marked difference in RMSD between the N- and C-terminal domains of the peptide indicates that the C terminus is less restricted. This is consistent with the notion of the embedding of the N-terminal region of gp41-FP in the hydrocarbon core of the micelle. Taking into consideration that the C-terminal residues of gp41-FP are more polar, our data indicate that the N terminus of gp41 inserts into the membrane as a helix but bends at residues A15 and G16, with the C-terminal portion of gp41-FP lying on the surface of the micelle.

Our NMR and CD data indicate that α-helix predominated in the SDS micelle solution, apparently at variance with the result of Nieva et al. for the peptide in POPG vesicular solution in which the β-conformation was observed by IR experiments (33). However, our CD data do not rule out the contribution of the β-form, since the helix content is approximately 59% in the presence of SDS micelles (Fig. 5) whereas the β-structure accounts for 26.7% of the population. Furthermore, the β-sheet is the major conformation of gp41-FP in aqueous solution (Fig. 4). The helical form is more easily observed in the NOE experiments in which short interproton distances are emphasized (21, 25). Therefore, the results presented here do not eliminate the possibility of a minor population of the peptide with β-sheet conformation that may not penetrate into the micelle. Our data also suggest that if at some stage(s) the fusion peptide inserts into the membrane, as supported by many experiments, it does so predominantly as a helix in the hydrophobic region of the bilayer. The observation

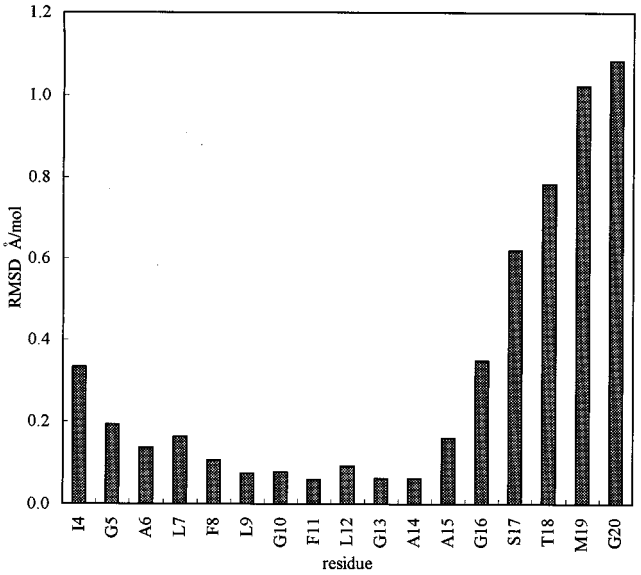

FIG. 12. RMSD (in angstroms per mole) plot for residues 4 to 20 of gp41-FP from 40 calculated structures. The dramatic increase in the RMSD value for residues following G16, illustrated by the splaying of the region in Fig. 11A, suggests that there is flexibility of the residue within the peptide in association with the SDS micelle and that the C-terminal region of the gp41-FP is free of the motional restriction from the micellar hydrocarbon chains.

that the helicity increases as the L/P ratio increases (36) suggests that helix is the vesicle-bound structure for the peptide, as a higher L/P ratio would mean more association of the peptide with the vesicle. The helical form has been proposed to correlate with the fusogenic activity of influenza virus HA2 peptide at acidic pH (26).

From the modeling results shown in Fig. 11 and 12, the divergence of the helix can be observed for the region following G16, demonstrating the flexibility of the residue. The larger RMSD values for the S17 to G20 region are not likely to arise from the fraying-end effect, because the region is not at the C terminus of gp41-FP and because the I4 to L7 stretch does not show RMSD values of similar magnitude. In combination with these modeling results, the spin-label attenuation experiments suggest that the FLG motif (Fig. 8 and 9; Table 3) is near the center of the micelle and that the A15 to G16 segment is located at the micelle-water interface with the C-terminal portion of gp41-FP close to the micellar surface (Table 3). A15 and G16 are absolutely conserved in all strains of HIV-1 and HIV-2 hitherto investigated (32), implying their importance in the function of the viral fusion peptide. Based on these results, a possible scenario for the role played by A15 to G16 in HIV-mediated fusion is proposed. Since they are located where the fusion peptide protrudes out into the bulk solution, the two residues may exert their biological function, among other possibilities, by the conformational flexibility conferred by the short side chain or absence of it for these two amino acids. For instance, the flexibility may facilitate the conformational change necessary for the pore formation (42) and lipid flow in the virus-mediated fusion. Moreover, these two residues have been implicated in the association with gp120 (11, 14). Thus, following the binding of gp120 to the cellular receptors (CD4 and CCR5 or fusin), the fusion peptides on the coiled-coiled oligomer of gp41 are exposed and may bend at the A15-G16 dipeptide and line the fusion pore between the viral and target cell membranes. The importance of G16 in syncytium formation by HIV-1 highlighted in the mutagenesis work of Delahunty et al. (11) may be partly explained by our finding. In particular, it is worth noting the dramatic difference in the effect of the Gly-to-Val mutation on the syncytium-inducing ability of the virus between G3, G5, and G20 on the one hand and G10, G13, and G16 on the other. The invariance of G10 and G13 may be ascribed to their role in initiating the helix (8), while the importance of G16 may reside in its flexibility at the water-micelle interface.

In summary, from CD and the spin-label-attenuated ^{1}H experiments, it was found that gp41-FP inserts into the SDS micelle primarily as a helix with A15 to G16 at the micelle-bulk solution interface. The insertion mode and helical structure have also been found for the peptide in the phospholipid solution. The residues following the flexible G16 are likely to adopt a distorted helical form and have substantial interaction with the micelle.

ACKNOWLEDGMENTS

S.F.C. and W.J.C. contributed approximately equivalently to this work.

We thank the National Science Council (NSC-85-2113-M001-037) and Academia Sinica of Republic of China for financial support.

We thank Shui-Tein Chen for synthesis of the tryptophan analog of fusion peptide of gp41 and Ming-Fai Tam for peptide characterization by mass spectrometry.

REFERENCES

1. **Bodenhausen, G., H. Kogler, and R. R. Ernst.** 1984. Selection of coherence-transfer pathways in NMR pulse experiments. J. Magn. Reson. **58:**370–388.
2. **Bosch, M. L., P. L. Earl, K. Fargnoli, S. Picciafuoco, F. Giombini, F. Wong-Staal, and G. Franchini.** 1989. Identification of the fusion peptide of primate immunodeficiency viruses. Science **244:**694–696.
3. **Brasser, R., M. Vandenbranden, B. Cornet, A. Burny, and J.-M. Ruysschaert.** 1990. Orientation into the lipid bilayer of an asymmetric amphipathic helical peptide located at the N-terminus of viral fusion protein. Biochim. Biophys. Acta **1029:**267–273.
4. **Braunschweiler, L., and R. R. Ernst.** 1983. Coherence transfer by isotropic mixing: application to proton correlation spectroscopy. J. Magn. Reson. **53:**521–528.
5. **Brown, L. R., C. Bosch, and K. Wüthrich.** 1981. Location and orientation relative to the micelle surface for glucagon in mixed micelles with dodecylphosphocholine. Biochim. Biophys. Acta **642:**296–312.
6. **Bullough, P. A., F. M. Hughson, J. J. Skehel, and D. C. Wiley.** 1994. Structure of influenza hemagglutinin at the pH of membrane fusion. Nature **371:**37–43.
7. **Cannon, B., C. F. Polnaszek, K. W. Butler, L. E. G. Eriksson, and I. C. P. Smith.** 1975. The fluidity and organization of mitochondrial membrane lipids of the brown adipose tissue of cold-adapted rats and hamsters as determined by nitroxide spin probes. Arch. Biochem. Biophys. **167:**505–518.
8. **Chang, D. K., W. J. Chien, and S. F. Cheng.** The FLG motif in the N-terminal region of gp41 of HIV-1 adopts a type-I ß turn in aqueous solution and serves as the initiation site for helix formation. Eur. J. Biochem., in press.
9. **Clague, M. J., J. R. Knutson, R. Blumenthal, and A. Herrmann.** 1991. Interaction of influenza hamagglutinin amino-terminal peptide with phospholipid vesicles: a fluorescence study. Biochemistry **30:**5491–5497.
10. **Davis, D. G., and A. Bax.** 1985. MLEV-17-based two-dimensional homonuclear magnetization transfer spectroscopy. J. Magn. Reson. **65:**355–360.
11. **Delahunty, M. D., I. Rhee, E. O. Freed, and J. S. Bonifacino.** 1996. Mutational analysis of the fusion peptides of the human immunodeficiency virus type 1: identification of critical glycine residues. Virology **218:**94–102.
12. **Dufourcq, J., and J.-F. Faucon.** 1977. Intrinsic fluorescence study of lipid-protein interactions in membrane models. Binding of melittin, an amphipathic peptide, to phospholipid vesicles. Biochim. Biophys. Acta **476:**1–11.
13. **Englander, J. J., D. B. Calhounn, and S. W. Englander.** 1979. Heat-stable enterotoxin of *Escherichia coli*: in vitro effects on guanylate cyclase activity, cyclic GMP concentration, and ion transport in small intestine. Proc. Natl. Acad. Sci. USA **75:**2800–2804.
14. **Freed, E. O., D. J. Myers, and R. Risser.** 1990. Characterization of the fusion domain of the human immunodeficiency virus type 1 envelope glycoprotein gp41. Proc. Natl. Acad. Sci. USA **87:**4650–4654.
15. **Gallaher, W. R.** 1987. Detection of a fusion peptide sequence in the transmembrane protein of human immunodeficiency virus. Cell **50:**327–328.
16. **Gallaher, W. R., J. P. Segrest, and E. Hunter.** 1992. Are fusion peptide really "sided" insertional helices? Cell **70:**531–532.
17. **Gething, M. J., R. W. Doms, D. Jork, and J. White.** 1986. Studies on the mechanism of membrane fusion: site specific mutagenesis of the hemagglu-

tinin of influenza virus. J. Cell Biol. **102:**11–23.
18. **Gordon, L. M., C. C. Curtain, Y. C. Zhong, A. Kirkpatrick, P. W. Mobley, and A. J. Waring.** 1992. The amino-terminal peptide of HIV-1 glycoprotein 41 interacts with human erythrocyte membranes: peptide conformation, orientation and aggregation. Biochim. Biophys. Acta **1139:**257–274.
19. **Havel, T. F., I. D. Kuntz, and G. M. Crippen.** 1983. The theory and practice of distance geometry. Bull. Math. Biol. **45:**665–720.
20. **Hennessey, J. P., Jr., and W. C. Johnson, Jr.** 1981. Informational content in the circular dichroism of proteins. Biochemistry **20:**1085–1094.
21. **Hurd, R. E.** 1990. Gradient-enhanced spectroscopy. J. Magn. Reson. **87:**422–428.
22. **Jeener, J., B. H. Meier, P. Bachmann, and R. R. Ernst.** 1979. Investigation of exchange process by two-dimensional NMR spectroscopy. J. Chem. Phys. **71:**4546–4553.
23. **Johnson, W. C.** 1990. Protein secondary structure and circular dichroism: a practical guide. Protein **7:**205–214.
24. **Kragh-Hansen, U., and T. Riisom.** 1976. Complexes of aliphatic sulfates and human-serum albumin studied by ^{13}C nuclear-magnetic-resonance spectroscopy. Eur. J. Biochem. **70:**15–23.
25. **Kumar, A., R. R. Ernst, and K. Wüthrich.** 1980. A two-dimensional nuclear overhauser enhancement (2D NOE) experiment for the elucidation of complete proton-proton cross-relaxation networks in biological macromolecules. Biochem. Biophys. Res. Commun. **95:**1–5.
26. **Lear, J. D., and W. F. DeGrado.** 1987. Membrane binding and conformational properties representing the NH_2 terminus of influenza HA-2. J. Biol. Chem. **262:**6500–6505.
27. **Leis, J., D. Baltimore, J. M. Bishop, J. Coffin, E. Flessiner, S. P. Goff, S. Oroslan, H. Robinson, A. M. Skalka, H. M. Temin, and V. Vogt.** 1988. Standardized and simplified nomeclature for proteins common to all retroviruses. J. Virol. **62:**1808–1809.
28. **Macura, S., Y. Huang, D. Suter, and R. R. Ernst.** 1981. Two-dimensional chemical exchange and cross-relaxation spectroscopy of coupled nuclear spins. J. Magn. Reson. **43:**259–281.
29. **Marion, D., and K. Wüthrich.** 1983. Application of phase sensitive two-dimensional correlated spectroscopy (COSY) for measurements of ^1H-^1H spin-spin coulping constants in proteins. Biochem. Biophys. Res. Commun. **113:**967–974.
30. **Mobley, P. W., C. C. Curtain, A. Kirkpatrick, M. Rostamkha, A. J. Waring, and L. M. Gordon.** 1992. The amino-terminal peptide of HIV-1 glycoprotein 41 lyses humanerythrocyte and CD4+ lymphocytes. Biochim. Biophys. Acta **1139:**251–256.
31. **Montagnier, L., F. Clavel, B. Krust, S. Chamaret, F. Rey, F. Barre-Sinoussi, and J. C. Chermann.** 1985. Identification and antigenicity of the major envelope glycoprotein of lymphadenopathy-associated virus. Virology **144:**283–289.
32. **Myers, G., S. Wain-Hobson, L. E. Henderson, B. Korber, K. T. Jeang, and G. N. Pavlakis.** ed. 1994. Human retroviruses and AIDS. Theoretical Biology and Biophysics Group 10, Los Alamos, N.M.
33. **Nieva, J. L., S. Nir, A. Muga, F. M. Goni, and J. Wilshut.** 1994. Interaction of the HIV-1 fusion peptide with phospholipid vesicles: different structural requirement for fusion and leakage. Biochemistry **33:**3201–3209.
34. **Nilges, M., G. M. Clore, and A. M. Gronnenborn.** 1988. Determination of three-dimensional structure of proteins from interproton distance data by hybrid distance geometry-dynamical simulated annealing calculations. FEBS Lett. **229:**317–324.
35. **Piotto, M., V. Saudek, and V. Sklenar.** 1992. Gradient-tailored excitation for single-quantum NMR spectroscopy of aqueous solutions. J. Biomol. NMR **2:**661–665.
36. **Rafalski, M., J. D. Lear, and W. F. DeGrado.** 1990. Phospholipid interactions of synthetic peptides representing the N-terminus of HIV gp41. Biochemistry **29:**7917–7922.
37. **Redfield, A. G., and S. D. Kuntz.** 1975. Quadrature Fourier NMR detection: simple multiplex for dual detection and discussion. J. Magn. Reson. **19:**250–254.
38. **Slepushkin, V. A., S. M. Andreev, M. V. Sidorov, G. B. Melikyan, V. B. Grigorriev, V. M. Chumakov, A. E. Grinfeldt, R. A. Manukyan, and E. V. Karamov.** 1992. Investigation of human immunodeficiency virus fusion peptides. Analysis of interrelations between their structure and function. AIDS Res. Hum. Retroviruses **8:**9–18.
39. **Solomon, I.** 1955. Relaxation processes in a system of two spins. Phys. Rev. **99:**559–565.
40. **Stegmann, T., J. M. Delfino, F. M. Richards, and A. Helenius.** 1991. The HA2 subunit of influenza hemagglutinin inserts into the target membrane prior to fusion. J. Biol. Chem. **266:**18404–18410.
41. **Steiner, R. F., and L. Garone.** 1991. The physical chemistry of biopolymer solutions, p. 192–193. World Scientific Publishing, Singapore.
42. **White, J. M.** 1992. Membrane fusion. Science **258:**917–924.
43. **Wishart, D. S., and B. D. Sykes.** 1994. Chemical shift as a tool for structure determination. Methods Enzymol. **239:**363–392.
44. **Wüthrich, K.** 1986. NMR of protein and nucleic acids. John Wiley & Sons, Inc., New York, N.Y.